Title

Virtual refrigerant charge sensing algorithm for residential CO_2 heat pumps

Journal

Applied Thermal Engineering, 302

ISSN

1359-4311

Authors

Guo, Fangzhou

Liang, Chenjiyu

Kim, Donghun

et al.

Publication Date

2026-08-01

DOI

10.1016/j.applthermaleng.2026.132139

Applied Thermal Engineering 302 (2026) 132139

Contents lists available at ScienceDirect

Applied Thermal Engineering

journal homepage: www.elsevier.com/locate/apthermeng

Research Paper

Virtual refrigerant charge sensing algorithm for residential CO_2 heat pumps

Fangzhou Guo [a], Chenjiyu Liang [a,*], Donghun Kim [a], Bo Shen [b], Yifeng Hu [b]

[a] Building & Industrial Energy Systems Division, Lawrence Berkeley National Laboratory, Berkeley, California, USA
[b] Building Technologies Research and Integration Center, Oak Ridge National Laboratory, Oak Ridge, TN, USA

ARTICLE INFO

Keywords:
Heat pump
Refrigerant charge
Fault detection and diagnosis
Virtual sensor
Energy efficiency

ABSTRACT

Natural refrigerants are increasingly adopted in next-generation heat pump systems, among which CO_2 heat pumps have attracted significant attention. However, due to their high operating pressures, the leakage risk is higher, resulting in undercharge conditions and degraded heat pump performance. Thus, developing an accurate refrigerant charge level detection technique is necessary to guarantee safe and efficient operation. Although virtual refrigerant charge (VRC) level calculation algorithms for CO_2 heat pumps exist, they typically rely on empirically selected features without a systematic selection framework, leading to multicollinearity and potential overfitting, which limit their prediction accuracy and generalizability. To address these issues, this study proposes a VRC algorithm framework with a systematic feature selection method that identifies physically meaningful and statistically significant features, and is applied using a residential CO_2 heat pump as a case study. The method is extended from previous work on conventional refrigerants to account for charge behavior in CO_2 gas coolers. The selected features include gas cooler outlet density, evaporator pressure, and superheat temperature. The results demonstrate that the proposed feature selection method significantly improves prediction accuracy compared to existing VRC approaches. A relatively small training dataset (~30 samples) is sufficient for feature identification and model development. The developed algorithm achieves less than 3% prediction error under both undercharge and overcharge conditions, representing reductions of 46.7% and 35.3% compared to two recent reference VRC algorithms for transcritical CO_2 heat pumps reported in the literature. The proposed algorithm and feature selection method enhance leakage detection capability, facilitate the deployment of CO_2 heat pump systems, and contribute to reduced energy waste and maintenance costs.

1. Introduction

Heat pumps play a crucial role in modern heating, ventilation, and air conditioning (HVAC) systems [1]. Their efficiency and reliability are strongly influenced by the refrigerant charge level [2]. Insufficient refrigerant charge can diminish heating or cooling output and raise energy consumption, whereas excessive charge may result in high pressures, lower efficiency, and even equipment damage [3–6]. Therefore, keeping the refrigerant charge within the appropriate range is essential to ensure the system operates efficiently, remains dependable, and has a long service life.

Directly measuring the refrigerant charge level in a heat pump system is difficult [7,8]. To address this, Li and Braun [9] proposed virtual refrigerant charge (VRC) sensor technology, which estimates the charge level using a linear regression model. This approach relies on subcooling and superheat temperatures as input features, as shown in Eq. (1), and has demonstrated reasonable accuracy for constant-speed heat pumps [9].

$$m_{charge} = c_0 + c_1 T_{sc} + c_2 T_{sh} \tag{1}$$

While detailed physics-based models can be used for simulation and, in principle, for state estimation, they are often computationally expensive and sensitive to uncertain parameters when deployed in real-time on residential heat pump controllers. In contrast, a VRC sensor provides a fast, closed-form charge estimate using measurements that are typically available in installed systems (pressure and temperature sensors). This enables near real-time monitoring of charge drift and supports early refrigerant-leak detection and maintenance, improving safety and operating efficiency with low implementation cost.

However, the accuracy of the previously described method declines as compressor speed varies in variable-speed heat pump applications. To overcome this limitation, Kim and Braun [10] introduced two additional features—refrigerant quality at the evaporator inlet and discharge superheat temperature—as shown in Eq. (2). Incorporating these variables reduced the charge level prediction error in heating mode from over

* Corresponding author.
E-mail address: ChenjiyuLiang@lbl.gov (C. Liang).

https://doi.org/10.1016/j.applthermaleng.2026.132139
Received 7 April 2026; Received in revised form 23 June 2026; Accepted 23 June 2026
Available online 25 June 2026

Nomenclature

c_0 to c_6	coefficients
$H_{dis,s}$	refrigerant enthalpy at the compressor outlet after isentropic compression, kJ/kg
H_{ei}	refrigerant enthalpy at the evaporator inlet, kJ/kg
H_{suc}	refrigerant enthalpy at the compressor inlet, kJ/kg
m_{charge}	refrigerant charge level, kg
m_r	refrigerant mass flow rate, kg/s
n	total number of data points
P_e	evaporator pressure, bar
P_g	gas cooler pressure, bar
$Power$	compressor power consumption, kW
$Speed_{rotation}$	compressor rotational speed, rpm
T_c	condensation temperature, °C
T_e	evaporation temperature, °C
T_{gi}	refrigerant temperature at gas cooler inlet, °C
T_{go}	refrigerant temperature at gas cooler outlet, °C
T_{gp}	refrigerant temperature at gas cooler pseudo-critical surface, °C
T_{sc}	subcooling temperature, °C
T_{sh}	superheat temperature, °C
T_{shd}	discharge superheat temperature, °C
Vol_{dis}	displacement volume, m^3/rev
x_{ei}	refrigerant quality at the evaporator inlet

Greek symbols

η_{is}	compressor isentropic efficiency
η_{vol}	compressor volumetric efficiency
ρ_{gi}	refrigerant density at gas cooler inlet, kg/m^3
$\overline{\rho}_{gi}$	nominal refrigerant density at gas cooler inlet, kg/m^3
ρ_{go}	refrigerant density at gas cooler outlet, kg/m^3
$\overline{\rho}_{go}$	nominal refrigerant density at gas cooler outlet, kg/m^3
ρ_{gp}	refrigerant density at gas cooler pseudo-critical surface, kg/m^3
ρ_{suc}	refrigerant density at compressor inlet, kg/m^3

Abbreviations

HCFC	hydrochlorofluorocarbon
HFC	hydrofluorocarbon
HFO	hydrofluoroolefin
HP	heat pump
HPDM	heat pump design model
HVAC	heating, ventilation, and air conditioning
HX	heat exchanger
MAPE	mean absolute percentage error
NTU	number of transfer unit
RMSE	root mean square error
VRC	virtual refrigerant charge

10% to 7% for heat pumps using R22 and R410A as refrigerants. These two mainstream algorithms have since been widely investigated and applied [11–15].

$$m_{charge} = c_0 + c_1 T_{sc} + c_2 T_{sh} + c_3 x_{ei} + c_4 T_{shd} \tag{2}$$

Beyond the features already discussed, other variables can also influence the refrigerant charge level. For instance, Boahen et al. [16] and Guo et al. [17] identified that both the evaporating and condensing temperatures of the heat pump system play a role. Because the mainstream methods typically determine the predictive charge level based on empirical knowledge, and since different refrigerants present different properties, the most suitable features for predicting refrigerant charge levels in heat pumps using different refrigerants remain unclear. Thus, based on the previous research, the possible features for heat pump charge level prediction are subcooling temperature, superheat temperature, refrigerant quality at the evaporator inlet, discharge superheat temperature, discharge saturation temperature, and suction saturation temperature [17], as shown in Eq. (3). This study uses a stepwise procedure to select the best set of features for the regression model.

$$m_{charge} = c_0 + c_1 T_{sc} + c_2 T_{sh} + c_3 x_{ei} + c_4 T_{shd} + c_5 T_c + c_6 T_e \tag{3}$$

For conventional hydrofluorocarbon (HFC) and hydrofluoroolefin (HFO) refrigerants, such as R410A, R290, and R454B [18], the stepwise feature selection method described in conjunction with Eq. (3) demonstrates strong adaptability for charge level prediction in variable-speed heat pumps [17,19]. However, CO_2 heat pumps operate under a transcritical refrigeration cycle with high operating pressures, which increases the risk of refrigerant leakage. The annual leakage rate can reach up to 15% [20,21], leading to significant degradation in heating capacity and system efficiency [22]. More importantly, the thermodynamic characteristics of transcritical CO_2 systems differ fundamentally from those of subcritical systems. In CO_2 heat pumps, a gas cooler replaces the condenser, and the refrigerant does not undergo phase change in this component [20]. As a result, key features commonly used in conventional VRC algorithms, such as subcooling temperature and discharge superheat temperature, are no longer available or physically meaningful. Therefore, the existing VRC formulations cannot be directly applied to CO_2 heat pumps, and further development of the VRC algorithm is required.

Jia et al. [23] employed four features, namely the gas cooler inlet temperature, gas cooler pressure, gas cooler outlet temperature, and evaporator temperature, to predict the charge level of the CO_2 heat pump using a neural network approach. Although machine learning–based methods can achieve good prediction performance, they generally require substantially larger training datasets and may suffer from overfitting and reduced interpretability, especially under limited-data conditions.

Building on the linear VRC algorithm presented in Eq. (2), a recent study from Zhang et al. [24] proposed two latest algorithms that utilize the refrigerant density at the inlet, outlet, and pseudo-critical surface of the gas cooler, along with features from the evaporator side, to predict the charge level of the CO_2 heat pump, as shown in Eqs. (4) and (5). It was reported that a 5% mean absolute error can be achieved.

$$m_{charge} = \begin{cases} c_0 + c_1\overline{\rho}_{go} + c_2\overline{\rho}_{gi} + c_3\rho_{gp} + c_4 T_{sh} + c_5 x_{ei} \ (T_{go} \le T_{gp}) \\ c_0 + \rho_{go} + c_2\rho_{gi} + c_3 T_{sh} + c_4 x_{ei} \ (T_{go} > T_{gp}) \end{cases} \tag{4}$$

$$m_{charge} = \begin{cases} c_0 + c_1\overline{\rho}_{go} + c_2\overline{\rho}_{gi} + c_3\rho_{gp} + c_4 T_{sh} \ (T_{go} \le T_{gp}) \\ c_0 + \rho_{go} + c_2\rho_{gi} + c_3 T_{sh} \ (T_{go} > T_{gp}) \end{cases} \tag{5}$$

Although the reference algorithms above are effective, the selection of appropriate features varies across different heat pump systems and capacities. Moreover, the features used in Eqs. (4) and (5) are often correlated, leading to redundancy and potential overfitting. The identification of an optimal feature set for charge level prediction is further complicated by the diversity in system configurations, particularly for CO_2 heat pumps. As a result, existing approaches are typically system-specific, and a generalized framework for feature selection is still lacking.

Therefore, this study develops a systematic feature-selection framework for VRC sensing in CO_2 heat pumps, rather than proposing another fixed regression equation. The novelty of this work lies in establishing a physics-guided and statistically constrained methodology for identifying physically meaningful and statistically significant features for refrigerant charge prediction. Building upon a previously developed approach for R410A heat pumps [17,19], the method is extended to residential CO_2 heat pump water heaters. The performance of the proposed framework is evaluated under both undercharge and overcharge conditions, demonstrating its advantages over state-of-the-art algorithms. In addition, the impact of training data sample size on feature selection and prediction accuracy is investigated. In practice, using the proposed method, the VRC coefficients can be identified using regression on limited experimental/field data, and the proposed feature-selection framework helps obtain a stable, physically consistent predictor without relying on empirically chosen features.

2. Feature selection method

This section introduces the proposed feature selection method. Rather than deriving a fixed equation for a specific system, the method establishes a generalized linear formulation with a set of candidate features. First, the relationships between key physical variables and the refrigerant charge level in a CO_2 heat pump are analyzed. Based on this analysis, a feature selection procedure is developed to identify physically consistent and statistically significant variables for charge level estimation.

2.1. Relationships between physical quantities

A commonly used residential CO_2 heat pump water heater is investigated in this study, as presented in Fig. 1(a). This system is operated under a transcritical heat pump cycle, as shown in Fig. 1(b), where there is a gas cooler instead of a condenser. Typically, temperatures and pressures on the refrigerant side are monitored via sensors, and the locations of these sensors are indicated in the diagram. This section analyzes the relationship between the measured or calculated physical quantities and the charge level.

Evaporator related features:

(1) Refrigerant quality at the evaporator inlet (x_{ei}): The refrigerant quality at the evaporator inlet typically shows a negative relationship with the charge level. This is because it is defined as the ratio of the mass of the gas phase to the total mass of the refrigerant mixture (including both gas and liquid phases) at the evaporator's entrance. A greater refrigerant quality at the inlet signifies a higher proportion of gas-phase refrigerant entering the evaporator, which means that the lower-density gas phase occupies a larger volume within the evaporator, resulting in a reduced charge level. The refrigerant quality can be calculated based on the evaporator inlet enthalpy (H_{ei}) and evaporation pressure (P_e). Since the expansion valve undergoes an isenthalpic throttling process, the evaporator inlet enthalpy (H_{ei}) remains identical to that at the gas cooler outlet. Therefore, variations in gas cooler outlet thermodynamic state and density directly affect the refrigerant quality at the evaporator inlet. Thus, it can be determined based on the measured gas cooler pressure (P_g) and outlet temperature (T_{go}), and it is necessary to use the proposed

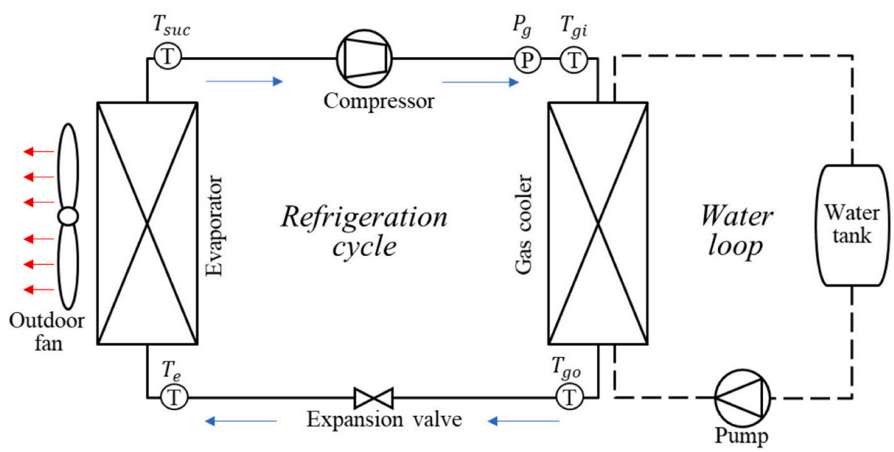

(a)

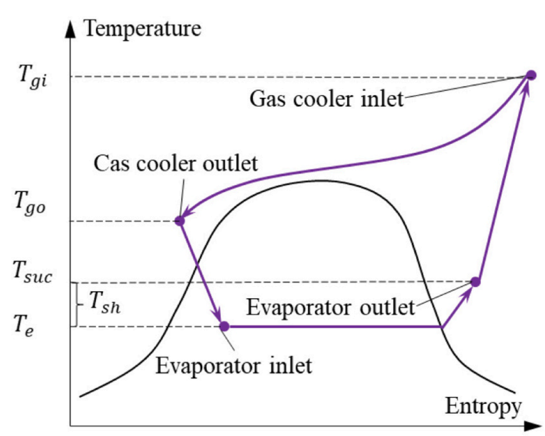

(b)

Fig. 1. Refrigerant charge level related physical quantities on (a) system diagram and (b) temperature-entropy diagram.

feature selection method (presented in Section 2.2) to identify the most suitable features.

(2) Evaporation pressure (P_e): The evaporation pressure generally exhibits a positive correlation with the charge level. When the system volume is fixed, an increase in the mass of the refrigerant results in a rise in system pressure. Consequently, a higher refrigerant charge level leads to an increase in the evaporation pressure.

(3) Superheat temperature (T_{sh}): The superheat temperature typically shows a negative correlation with the charge level. In the evaporator, the refrigerant is present in both two-phase and gas phase. A higher superheat temperature indicates a greater proportion of superheated gas-phase refrigerant. Since gas-phase refrigerant is the least dense, this relationship suggests that an increase in superheat temperature corresponds to a lower charge level.

Gas cooler related features:

(1) Gas cooler outlet density (ρ_{go}): Gas cooler outlet density shows a positive relationship with the charge level, since the gas cooler has a fixed internal volume, meaning a higher refrigerant charge level must manifest as increased refrigerant density. Gas cooler outlet density can be calculated based on the gas cooler outlet temperature (T_{go}) and gas cooler pressure (P_g).

(2) Gas cooler pseudo-critical density (ρ_{gp}): The gas cooler pseudo-critical density means the density at the pseudo-critical surface at the gas cooler, which shows a positive relationship with the charge level. Notably, the variation rate of CO_2 density peaks at a specific temperature for a given pressure. For analytical convenience, the locus of maximum density gradients across varying pressures is defined as the pseudo-critical surface [24], as shown in Fig. 2. Therefore, the pseudo-critical density refers to the refrigerant density evaluated at this pseudo-critical surface. As illustrated in Fig. 2, the density variation is most sensitive in the pseudo-critical region. Thus, Ref. [24] proposed the pseudo-critical density as a feature for refrigerant charge estimation. The pseudo-critical density (ρ_{gp}) can be obtained based on pseudo-critical temperature (T_{gp}), which is related to the gas cooler pressure (P_g), as shown in Eqs. (6) and (7).

$$T_{gp} = 0.21P_g + 22.1 \tag{6}$$

$$\rho_{gp} = 2.96T_{gp} + 365.8 \tag{7}$$

(3) Gas cooler inlet density (ρ_{gi}): Similarly, gas cooler inlet density shows a positive relationship with the charge level, and can be calculated based on the gas cooler inlet temperature (T_{gi}) and gas cooler pressure (P_g).

In summary, the relationships between the six physical variables as candidate features and the refrigerant charge level are summarized in Table 1. Furthermore, under the same operating conditions, Fig. 3 compares the refrigeration cycles at the nominal refrigerant charge and in the undercharge condition after a refrigerant leak. After a significant refrigerant leak, the entire refrigeration cycle shifts to the right in the temperature-entropy diagram (reflecting lower refrigerant density and reduced system pressure), exhibiting a higher superheat temperature and low pressure.

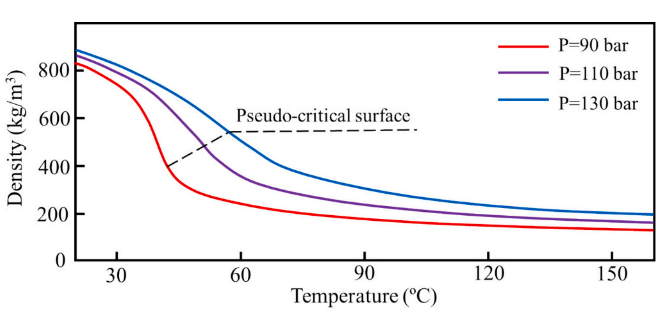

Fig. 2. Density and temperature distribution in gas cooler [24].

2.2. Feature selection method

Based on the analysis in Section 2.1, six physical quantities are considered as the candidate features for charge level prediction. The charge level prediction is considered a linear regression model, as shown in Eq. (8).

$$m_{charge} = c_0 + c_1\rho_{go} + c_2\rho_{gp} + c_3\rho_{gi} + c_4x_{ei} + c_5P_e + c_6T_{sh} \tag{8}$$

The six physical quantities are candidates, which means they don't have to be selected eventually. After the feature selection method presented in Fig. 4, the appropriate features are determined for charge level prediction.

In this study, a stepwise approach is employed to identify the optimal set of features for the regression model. The process is termed forward selection, which begins with a linear regression model containing no features and incrementally adds one feature at a time. For each feature introduced, its p-value is calculated using the training dataset to assess its statistical significance for charge level prediction. A p-value threshold of 0.05 is adopted, with values below this limit indicating that the feature is statistically significant. The process ends when no more features are needed for the linear regression model. By this means, only features that significantly impact the charge level are selected.

Additionally, the algorithm verifies whether the corresponding coefficients, i.e., c_1 to c_6 in Eq. (8), are consistent with the physical principles of the CO_2 heat pump system. Only coefficients consistent with physical laws will be selected, and they must align with the signs of the coefficients specified in Table 1.

3. Evaluation method

To develop and validate VRC algorithms for predicting the charge level in CO_2 heat pumps, this study utilizes a simulation model of a residential CO_2 heat pump water heater, as illustrated in Fig. 1, to generate system performance data across a range of heating conditions. Noise is then added to the simulated data to emulate sensor uncertainty and operational fluctuations within the system, which are subsequently divided into training and testing subsets. Specifically, the noise levels (maximum deviations) are set to 0.01 kg (10 g) for refrigerant charge, 2 bar for pressure, and 1 °C for temperature, reflecting typical measurement errors and ambient perturbations. The training data are used to identify suitable features and construct the developed algorithm. In turn, the testing data are employed to evaluate the algorithm's adaptability and accuracy in estimating the charge level under various operating conditions, as shown in Fig. 5.

3.1. Numerical model for simulation

The heat pump simulation model is employed to generate various operating performances for the development and evaluation of the algorithms. In this study, the DOE/ORNL Heat Pump Design Model (HPDM) developed by Oak Ridge National Laboratory [25] is used as the simulation tool to produce different heating operation conditions for a residential two-speed (2400 and 3600 rpm) CO_2 heat pump water heater, which has a nominal heating capacity of approximately 40,000 Btu/h (12 kW), and a nominal charge level of 3.9 lb. (1.77 kg).

The HPDM is a public-domain platform that is free to use for designing and modeling HVAC equipment under steady-state and quasi-

Table 1
The signs of the coefficients for different physical variables in predicting the charge level.

Possible Features	Gas cooler outlet density	Gas cooler pseudo-critical density	Gas cooler inlet density	Refrigerant quality at the evaporator inlet	Evaporator pressure	Superheat temperature
Coefficients	c_1	c_2	c_3	c_4	c_5	c_6
Sign*	+	+	+	–	+	–
Required sensors	Gas cooler pressure and outlet temperature	Gas cooler pressure	Gas cooler pressure and inlet temperature	Gas cooler pressure and outlet temperature, evaporator inlet temperature	Evaporator inlet temperature	Evaporator inlet and outlet temperatures

[*] Positive and negative correlations are represented as "+" and "–", respectively.

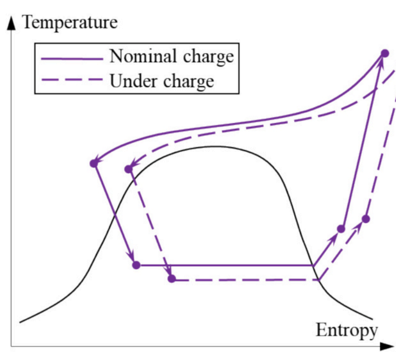

Fig. 3. Refrigeration cycle at nominal-charge and under-charge conditions.

steady-state conditions. It is widely utilized by engineers, academics, and equipment manufacturers, and has been validated against experimental results [2,26]. This study highlights several key features of the HPDM, as outlined below.

- Extensive Component Library: A library of hundreds of component models that simulate the detailed behavior of most heat exchangers, compressors, fans, pumps, expansion devices, and connection lines.
- Hardware-Based Modeling: Users can define physical hardware components such as heat exchangers (specifying type, size, fin pitch, etc.), air flow parameters, and compressor selections. In terms of heat exchanger modeling, it supports arbitrary tube connections and simulates both refrigerant and air flow paths using a segment-to-segment approach.
- Comprehensive Fluid Property Handling: HPDM manages the properties of a wide range of fluids, including air, water, glycol, as well as refrigerants such as hydrochlorofluorocarbon (HCFC), HFC, new HFO, and natural refrigerants like CO_2 and propane.

3.1.1. Compressor model

To model the supercritical CO_2 heat pump water heater, the compressor model is efficiency-based with inputting measured isentropic and volumetric efficiencies. The volumetric efficiency is defined in Eq. (9), and the isentropic efficiency is shown in Eq. (10).

$$m_r = Vol_{dis} \times Speed_{rotation} \times \rho_{suc} \times \eta_{vol} \tag{9}$$

$$Power = m_r \times \left(H_{dis,s} - H_{suc}\right) / \eta_{is} \tag{10}$$

where, η_{vol} is compressor volumetric efficiency, which is considered as 0.95 in this study; η_{is} is compressor isentropic efficiency, which is considered as 0.7 in this study [27,28]; H_{suc} is compressor suction enthalpy; $H_{dis,s}$ is the enthalpy obtained at the compressor discharge pressure and suction entropy. Here, fixed compressor efficiencies are assumed because detailed compressor performance maps are not available for the studied system. Future work may incorporate map-based efficiency correlations when such data become available.

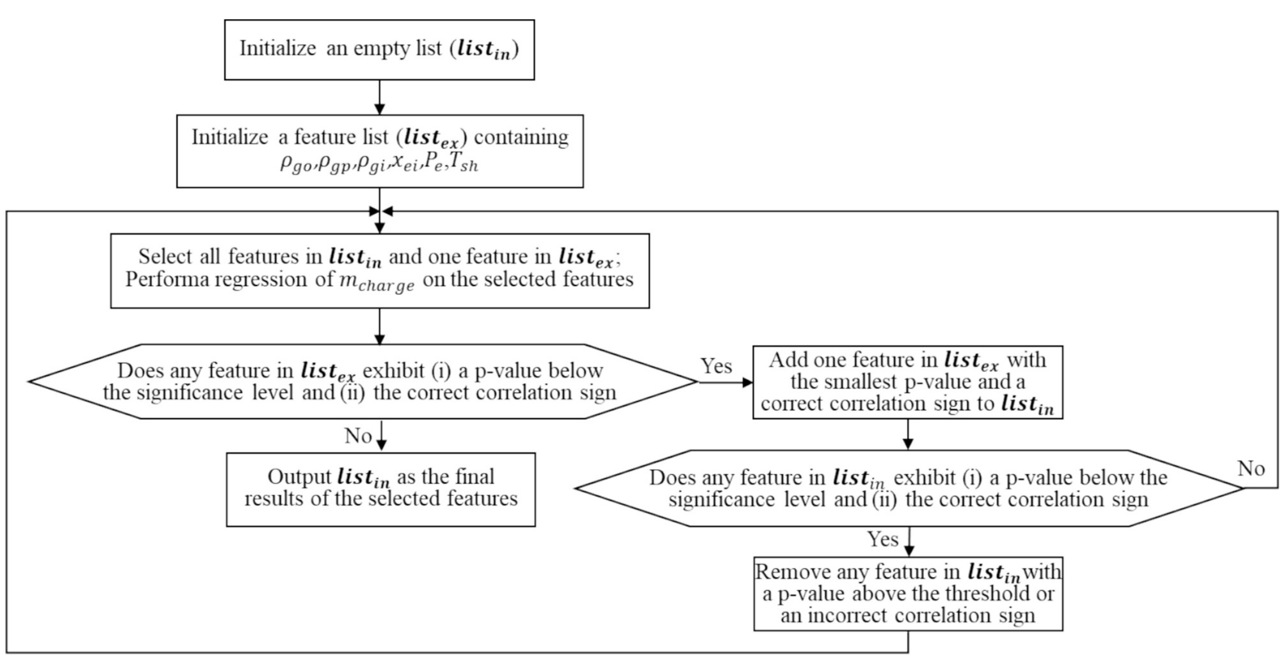

Fig. 4. Refrigerant charge level related feature selection method.

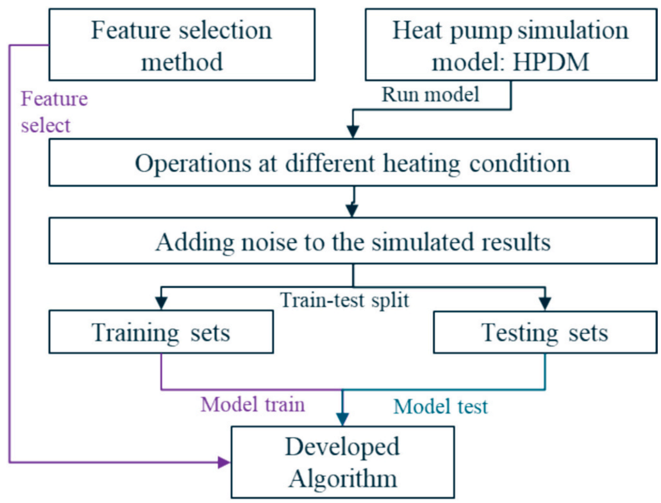

Fig. 5. Principle of virtual refrigerant charge sensor development and evaluation.

3.1.2. Evaporator model

A fin-and-tube coil (FTC) heat exchanger serves as the evaporator for the CO_2 heat pump water heater. A segment-to-segment modeling approach can be employed to model FTC heat exchangers by dividing each tube into multiple segments, as illustrated in Fig. 6. Air side temperature and humidity mix between the upstream two neighboring tubes and enter the following middle tube. It considers phase change in each segment and calculates local heat transfer and pressure drop. The coil model accumulates refrigerant charge in individual segments, separately for vapor, liquid, and two-phase, depending on local refrigerant temperature, pressure, quality, and mass flux. In the refrigerant two-phase region, the Hughmark model [29] is adopted to calculate segmental void fraction and two-phase density.

In the case of water condensing on an evaporating coil, both heat and mass transfer need to be considered. The approach for modeling a wet coil is based on Braun [30]. Braun [30] introduced the parameter of the air saturation specific heat at the refrigerant temperature to model wet coils. Using the air saturation specific heat, the existing effectiveness relationships developed for sensible heat transfer can also be used for heat and mass transfer, based on the modified definitions for the number of transfer units and capacitance rate ratio. The driving potential for heat transfer in the case of a wet coil is the difference between the enthalpies of the inlet air and the saturated air enthalpy at the refrigerant temperature.

3.1.3. Gas cooler model

For gas coolers in the CO_2 heat pump, common refrigerant-to-water heat exchangers contain brazed plate heat exchangers and twisted tube-in-tube heat exchangers. They are modelled using equations similar to those used for refrigerant-to-air heat exchangers for sensible heat transfer. The segment-to-segment modeling approach is adopted, which divides individual refrigerant-to-water flow channels into numerous control volumes, as shown in Fig. 7. The effectiveness-NTU method [31] is used. Channel hydronic flow diameter is used for local heat transfer and void fraction calculations.

In this study, the CO_2 heat pump water heater is designed to use a brazed plate heat exchanger as its gas cooler, operating within the supercritical region. The correlations for heat transfer and pressure drop are based on the single vapor phase, with the local density determined as a function of both pressure and temperature. The CO_2-side gas cooler heat transfer coefficient was calculated using the Dittus–Boelter correlation for single-phase supercritical flow [32], while the refrigerant thermophysical properties were evaluated using CO_2 properties under transcritical operating conditions.

3.1.4. Model validation

The HPDM model used in this study has been validated using previously collected experimental data from an R410A heat pump system to demonstrate the validity of its model structure and governing eqs. [2]. The validation was conducted under a wide range of heating conditions, including varying compressor speeds, electronic expansion valve (EXV) opening steps, outdoor temperatures, and refrigerant charge levels, as summarized in Table 2.

The validation results are presented in Fig. 8, showing good agreement between the experimental measurements and simulation results. This agreement indicates that the underlying thermodynamic modeling framework and governing equations of the HPDM are reasonable and reliable.

Furthermore, based on the same modeling framework, the present study replaces the refrigerant from R410A with CO_2 while maintaining the same model structure and solution methodology. Therefore, the previously validated modeling framework provides a basis for

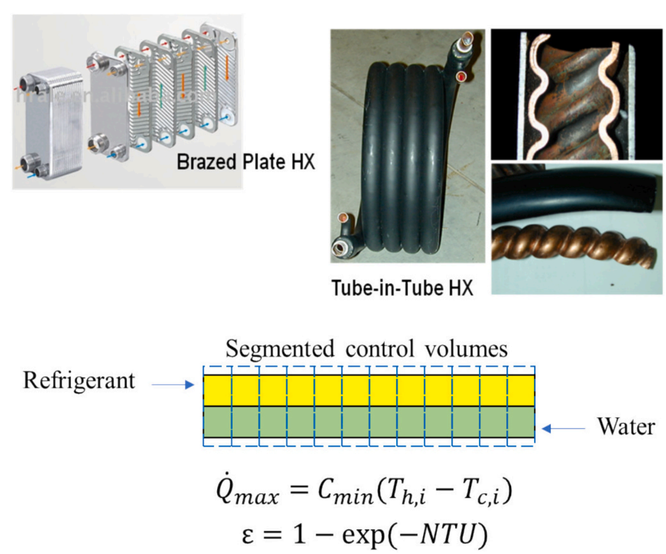

Fig. 7. Gas cooler model: segment-to-segment modeling approach for refrigerant-to-water heat exchangers.

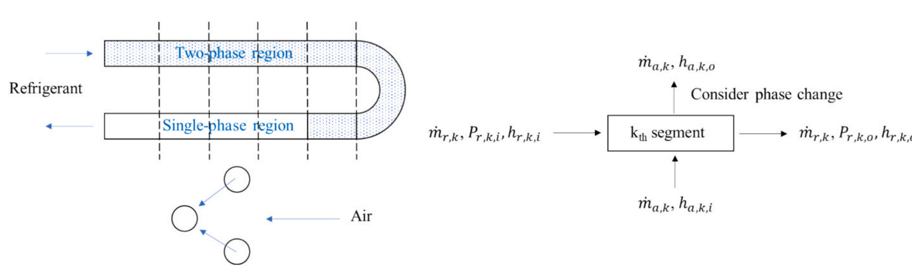

Fig. 6. Evaporator model: segment-to-segment modeling approach for fin-and-tube coil.

Table 2
Experiment conditions for model validation.

Variable	Compressor speed	Refrigerant flow rate	EXV steps	Indoor temperature	Outdoor temperature	Charge level
Unit	rpm	m^3/s	/	°C	°C	kg
Range	1300–3200	0.226–0.566	100–240	21.1	8.3–12.5	4.4–6.2

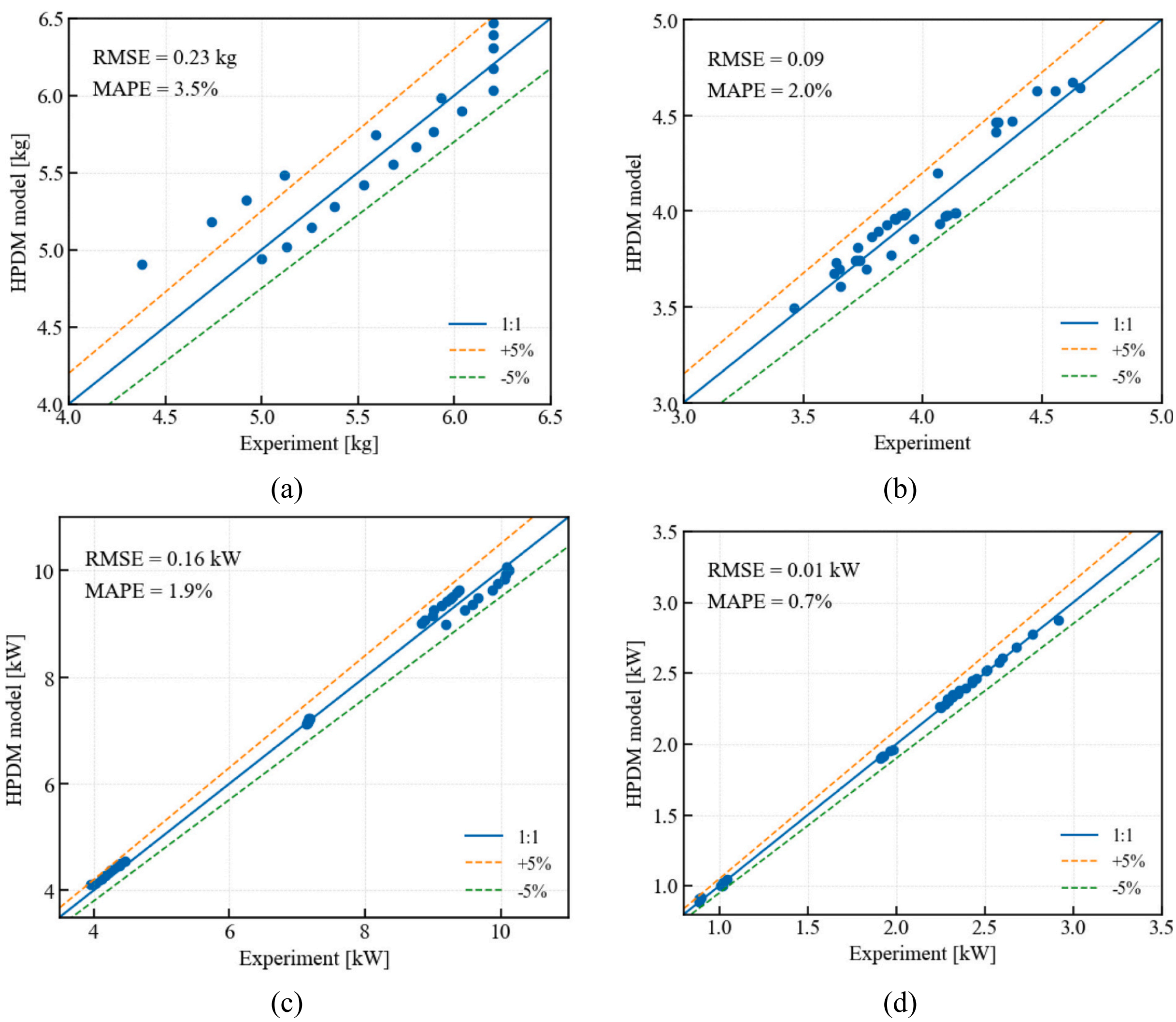

Fig. 8. Validation of the HPDM model: (a) charge level; (b) COP; (c) heating capacity; (d) power consumption.

generating simulation data for algorithm development and comparative evaluation. However, dedicated experimental validation is still needed to assess the applicability of the framework to transcritical CO_2 heat pump systems.

3.2. Performance evaluation method

According to AHRI Standard 550/590–2020 (I—P) [33], the heating conditions listed in Table 3 are selected for CO_2 heat pump performance simulation, as well as for algorithm training and testing. For each heating condition, the superheat temperature, discharge pressure, and compressor speed are varied as input parameters to the HPDM model,

Table 3
Simulation conditions chosen for charge level predictions.

Condition	Evaporator Air Inlet Temperature (°F/°C)	Gas Cooler Water Inlet Temperature (°F/°C)	Superheat Temperature (°F/°C)	Discharge Pressure (psi/Bar)	Compressor speed (rpm)
1	60/15.6	100 to 130/37.8 to 54.4	4 to 24/2.2 to 13.3	1600 to 2100/110.3 to 144.8	3600/2400
2	50/10.0				
3	40/4.4				
4	30/−1.1				
5	20/−6.7				
6	15/−9.4				

thereby generating different charge levels within the heat pump cycle. A total of 851 datasets were generated. First, 100 datasets were randomly selected as a fixed test set. The remaining 751 datasets formed the training pool. To investigate the effect of training size, subsets containing 20, 30, 50, and 100 samples were randomly selected from the training pool. Unless otherwise specified, the feature-selection results presented in Table 4 were obtained using the 30-sample training set, because practical applications typically have limited training data. All testing results were evaluated using the same fixed 100-sample test set.

After simulating the CO_2 heat pump water heater performance using the HPDM model under various heating conditions, the results are added with evenly distributed noise considering the sensors' uncertainties. Specifically, this noise is generated with a mean of zero and specified maximum deviations for each relevant variable in the dataset. The noise levels are defined as follows: a maximum deviation of 0.01 kg (10 g) for charge level, 2 bar for pressure, and 1 °C for temperature; these are selected based on the accuracy specifications of commercially available pressure and temperature sensors commonly used in CO_2 heat pump systems. By adding this generated noise to the selected variables, the process effectively simulates measurement errors and operational variability inherent in the heat pump system. This results in a more realistic dataset, enhancing the robustness of the developed algorithm during the training phase. Then, the developed algorithm is trained using the standardized simulation results and the feature selection method.

Subsequently, after the algorithm development, the accuracy of both the developed algorithm and the two reference algorithms is evaluated and tested. The root mean square error (RMSE) and mean absolute percentage error (MAPE) are employed as metrics to assess the prediction accuracy of the algorithms for charge level calculation, as shown in Eqs. (11) and (12).

$$RMSE = \sqrt{\frac{1}{n}\sum_{i=1}^{n}\left(m_{charge,i} - \widehat{m}_{charge,i}\right)^2} \tag{11}$$

$$MAPE = \frac{1}{n}\sum_{i=1}^{n}\left|\frac{m_{charge,i} - \widehat{m}_{charge,i}}{m_{charge,i}}\right| \tag{12}$$

where, n is the total number of data points, and $m_{charge,i}$ and $\widehat{m}_{charge,i}$ are the actual and predicted values of charge level for the ith data point.

4. Results and discussion

This section first presents the simulation data to demonstrate the reasonableness of the model and illustrates the correlations between the candidate features and the refrigerant charge level. It then presents the feature selection results and evaluates the performance of the developed algorithm using the feature selection method and compares it with the performances of the reference algorithms. Finally, limitations are discussed.

4.1. Simulation results

In this study, an experimentally validated HPDM model was used to generate 851 simulation results under varying operating conditions, including refrigerant charge level, compressor speed, outdoor air temperature, water inlet temperature, as well as superheat and discharge pressure.

Table 4
Selected features and p-values obtained using the 30-sample training set.

Selected features	ρ_{go}	P_e	T_{sh}
Explanation	Gas cooler outlet density	Evaporator pressure	Superheat temperature
Coefficients	0.23	0.13	−0.17
P-values	4.70e-24	4.23e-17	1.02e-19

This section first presents the simulation results at the nominal charge level of 1.77 kg under typical operating conditions, with an outdoor temperature of 45 °F (7.2 °C) and a water inlet temperature of 130 °F (54.4 °C), as shown in Fig. 9.

A Pearson correlation was conducted to evaluate the relationship between candidate variables and the refrigerant charge, based on a dataset of 851 simulation results, as shown in Fig. 10. The results indicate that the refrigerant charge is strongly positively correlated with ρ_{gi} (0.76) and ρ_{go} (0.61), suggesting that density-related variables play a dominant role in determining the system charge. In contrast, x_{ei} (−0.73) and T_{sh} (−0.56) exhibit strong negative correlations with charge, indicating that higher vapor quality and superheat are associated with lower refrigerant charge levels. In addition, P_e (0.52) and ρ_{gp} (0.38) show a moderate positive correlation with the refrigerant charge. The relationships between the variables and the refrigerant charge level are consistent with the analysis presented in Section 2. Additionally, a very strong negative correlation is observed between x_{ei} and ρ_{go} (−0.95), implying significant multicollinearity between these variables. Therefore, it is not advisable to include both variables simultaneously in the regression model. These findings provide physical insight into the system behavior and guide the feature selection process for the regression model.

4.2. Feature selection results

Sections 4.2 and 4.3 first present the results obtained using the 30-sample training set. This sample size was selected because practical applications typically have limited experimental data available for model development. The performance of the proposed algorithm is compared with that of the reference algorithms under this training size. The effects of different training data sizes on feature selection and charge level prediction accuracy are subsequently discussed in Section 4.4.

By applying the feature selection method described in the Methodology section to the training data under various heating conditions, gas cooler outlet density, evaporator pressure, and superheat temperature are identified as the selected features, and all of them present the correct coefficients and statistically significant p-values, as shown in Table 4. Consequently, the developed algorithm incorporates these three variables, as presented in Eq. (13). Since the refrigerant is primarily distributed in the gas cooler and evaporator, this algorithm can accurately reflect the charge level throughout the heat pump cycle.

$$m_{charge} = c_0 + c_1\rho_{go} + c_2P_e + c_3T_{sh} \tag{13}$$

The features not selected are presented in Table 5, which include the evaporator inlet quality, inlet and pseudo-critical densities of the gas cooler. They are not selected because their p-values are greater than the criterion of 0.05, thus they are not statistically significant for charge level prediction.

4.3. Algorithm performance

Based on Eq. (8), the algorithm was trained and tested across a range of heating conditions, with varying compressor speed, superheat temperature, discharge pressure, and charge level. The training RMSE was 0.070 lb. (0.032 kg), the MAPE was 1.47%, and the testing RMSE and MAPE were 0.112 lb. (0.051 kg) and 2.57%, respectively, as illustrated in Fig. 11. The above describes that the overall RMSE and MAPE include both overcharge and undercharge scenarios. In practical applications, more emphasis is placed on the undercharge situation caused by refrigerant leakage after the equipment is installed and operated. It can be seen that the algorithm can still ensure an error within 10% even when the refrigerant leakage amount exceeds 20% of the nominal charge.

Based on Eqs. (4) and (5), the other two reference algorithms were

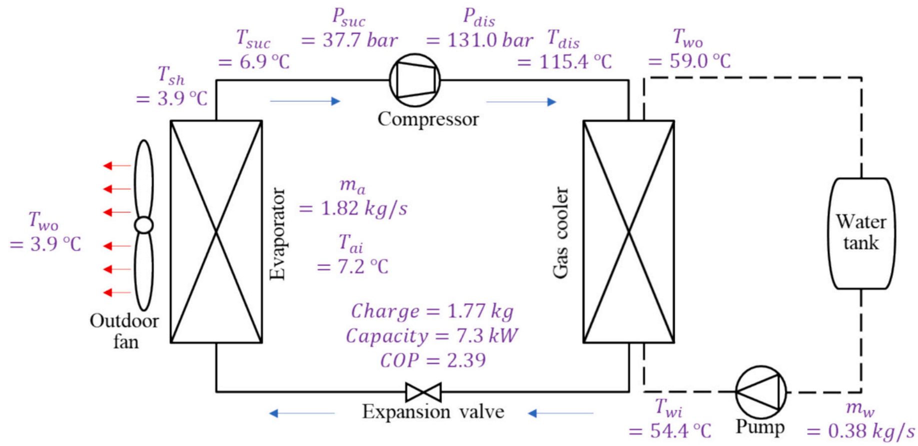

Fig. 9. Performance under a typical operating condition.

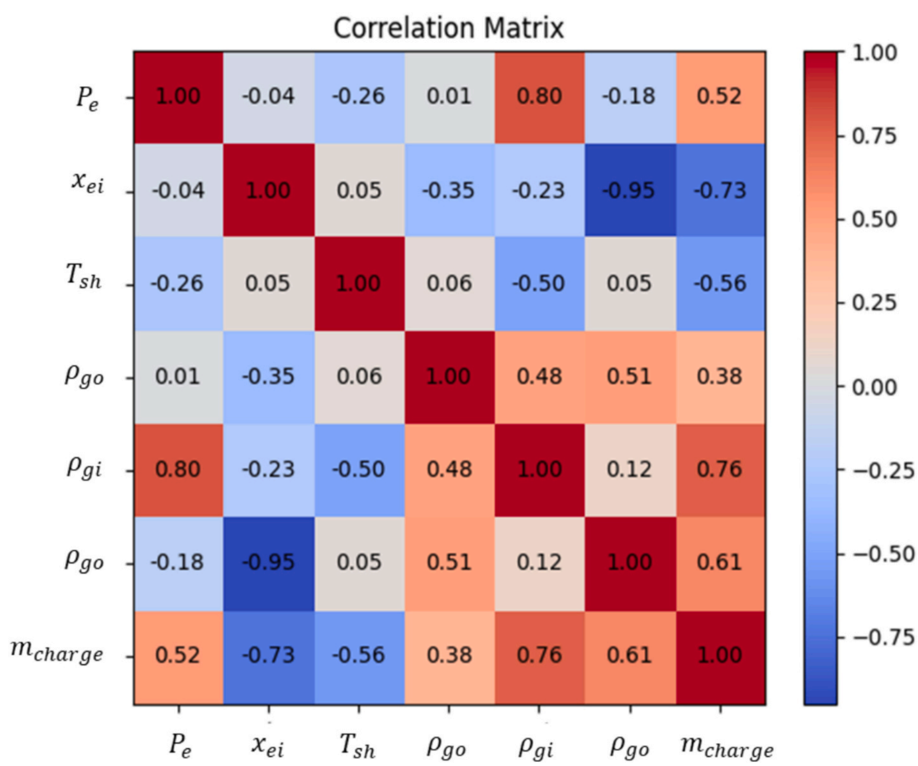

Fig. 10. Correlation matrix between features and charge level.

Table 5
Non-selected features and p-values obtained using the 30-sample training set.

Non-selected features	x_{ei}	ρ_{gp}	ρ_{gi}
Explanation	Refrigerant quality at the evaporator inlet	Gas cooler pseudo-critical density	Gas cooler inlet density
P-values	3.35e-01	8.32e-01	6.15e-01

trained under various heating conditions with different charge levels.

For reference algorithm 1 proposed by Zhang et al. [24] (presented in Eq. (4)), the training results are presented in Table 6. It can be observed that, without applying the proposed feature selection and directly adopting empirically selected features, the regression results are not consistent with the underlying physical behavior. For instance, the coefficients of the density variables ρ_{gp} and ρ_{go} are negative, which contradicts their physical interpretation. Furthermore, several features exhibit p-values significantly higher than the threshold of 0.05, indicating a lack of statistical significance. The training RMSE and MAPE were 0.065 lb. (0.030 kg) and 1.31%, and the testing RMSE was 0.206 lb. (0.094 kg), the MAPE was 4.82%, respectively, for the reference algorithm 1 in Eq. (4), as shown in Fig. 12. Therefore, although the method achieves a low training error, it does not perform well on the test dataset.

For reference algorithm 2 proposed by Zhang et al. [24] (presented in Eq. (5)), the training results are presented in Table 7. Similar to reference algorithm 1, the training results of reference algorithm 2 show that the coefficient of the density variable ρ_{gp} is negative, which is inconsistent with its physical interpretation. However, all variables are statistically significant. The training RMSE and MAPE were 0.068 lb.

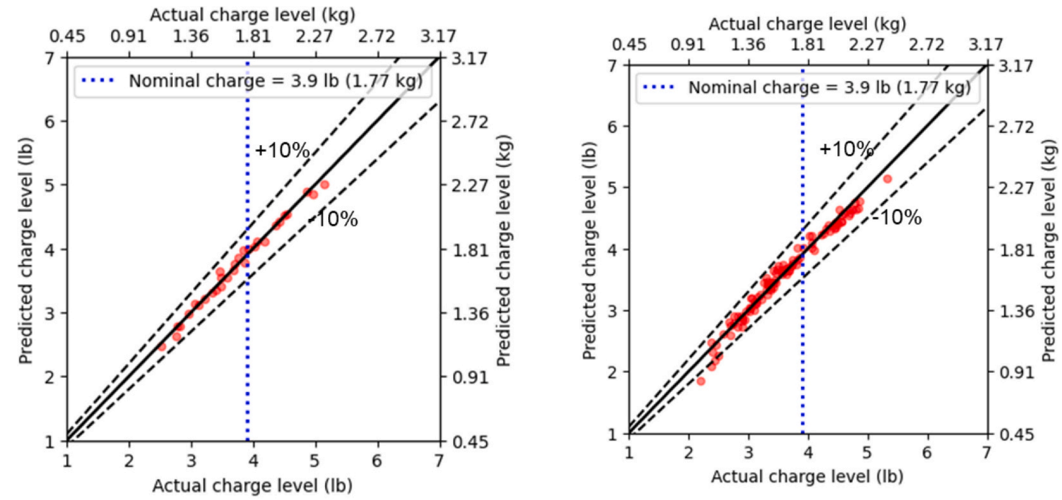

(a) (b)

Fig. 11. Developed algorithm's performance: (a) training; (b) testing.

Table 6
Coefficients and p-values of reference algorithm 1 using the 30-sample training set.

Features when $T_{go} \le T_{gp}$	$\overline{\rho}_{go}$	$\overline{\rho}_{gi}$	ρ_{gp}	T_{sh}	x_{ei}
Explanation	Gas cooler nominal outlet density	Gas cooler nominal inlet density	Gas cooler pseudo-critical surface density	Evaporator superheat	Evaporator inlet quality
Coefficients	0.21	0.21	−0.05	−0.06	−0.0004
P-values	1.84e-02	3.59e-04	1.18e-02	1.81e-02	9.94e-01
Features when $T_{go} > T_{gp}$	ρ_{go}	ρ_{gi}	T_{sh}	x_{ei}	
Explanation	Gas cooler outlet density	Gas cooler inlet density	Evaporator superheat	Evaporator inlet quality	
Coefficients	−0.03	0.08	−0.14	−0.19	
P-values	8.36e-01	1.33e-01	9.77e-03	2.88e-01	

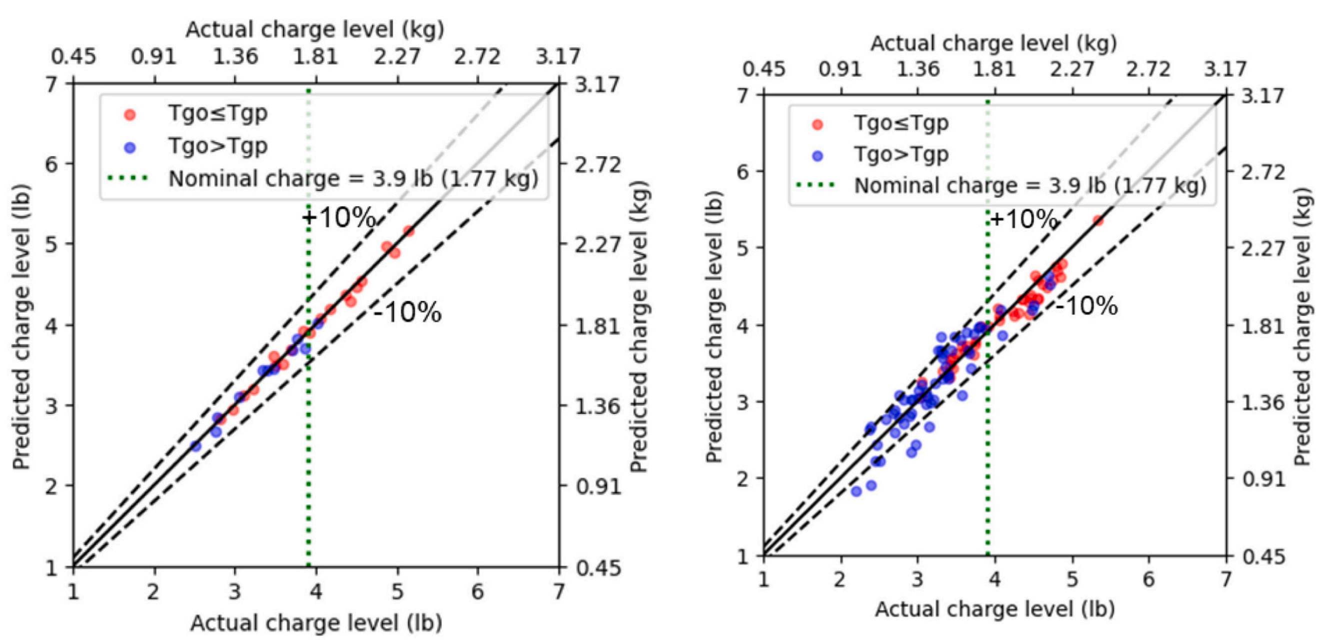

(a) (b)

Fig. 12. Reference algorithm 1's performance: (a) training; (b) testing.

(0.031 kg) and 1.33%, and the testing RMSE and MAPE were 0.166 lb. (0.075 kg) and 3.97%, respectively, for the reference algorithm 2

Table 7
Coefficients and *p*-values of reference algorithm 2 using the 30-sample training set.

Features when $T_{go} \le T_{gp}$	$\overline{\rho}_{go}$	$\overline{\rho}_{gi}$	ρ_{gp}	T_{sh}
Explanation	Gas cooler nominal outlet density	Gas cooler nominal inlet density	Gas cooler pseudo-critical surface density	Evaporator superheat
Coefficients	0.21	0.21	−0.05	−0.06
P-values	3.50e-11	8.76e-11	1.35e-04	8.79e-05
Features when $T_{go} > T_{gp}$	ρ_{go}	ρ_{gi}	T_{sh}	
Explanation	Gas cooler outlet density	Gas cooler inlet density	Evaporator superheat	
Coefficients	0.12	0.12	−0.11	
P-values	1.99e-03	8.17e-04	4.12e-03	

presented in Eq. (5), as shown in Fig. 13. Compared with reference algorithm 1, reference algorithm 2 excludes x_{ei}, which exhibits strong correlations with other variables. This reduces multicollinearity and mitigates overfitting, leading to improved performance on the test dataset.

The testing MAPEs comparison between the developed algorithm by the proposed feature selection method and the two reference algorithms proposed by Zhang et al. [24] (presented in Eqs. (4) and (5)) is presented in Table 8. The developed algorithm achieves an MAPE of 2.57% on the test dataset, demonstrating a substantial improvement over the reference algorithms. The prediction error is reduced by 46.7% compared to reference algorithm 1 and by 35.3% compared to reference algorithm 2. This improvement can be attributed to the use of an appropriate feature selection strategy. By selecting physically meaningful features and avoiding strong correlations among variables, the proposed method reduces multicollinearity and mitigates overfitting. As a result, the model achieves more accurate predictions on unseen data.

Table 8
Testing MAPEs of different algorithms evaluated using the fixed 100-sample test set.

Algorithm	MAPE in testing	Improvement
Developed	2.57%	46.7% (vs Reference 1) 35.3% (vs Reference 2)
Reference 1	4.82%	/
Reference 2	3.97%	/

4.4. Discussion

In the results section, the algorithm is trained using 30 operating conditions. This section discusses the impact of varying training data sizes on the algorithm's performance.

The selected features with their *p*-values under different training data sizes are presented in Table 9. As the sample size increases, the p-values of the features decrease. When the training sample size is 20, the selected features differ from those obtained with larger sample sizes (the selected data are subject to randomness). Once the sample size reaches 30, the selected feature set remains unchanged with further increases in sample size.

The test MAPEs under different training data sample sizes for the developed and the reference algorithms are presented in Eqs. (4) and (5) are shown in Table 10. The developed algorithm consistently outperforms the reference algorithms across all training sizes, especially under small-sample conditions. For example, when the training size is

Table 9
Selected features' p-values under different training data sizes.

Feature	Training data size of 20	Training data size of 30	Training data size of 50	Training data size of 100
T_{gco}	Not selected	4.70e-24	4.03e-37	1.86e-73
P_{gc}	Not selected	Not selected	Not selected	Not selected
T_{gci}	5.51e-09	Not selected	Not selected	Not selected
x_{ei}	5.76e-14	Not selected	Not selected	Not selected
P_e	Not selected	4.23e-17	7.73e-29	1.44e-56
T_{sh}	1.20e-08	1.02e-19	2.00e-29	6.68e-53

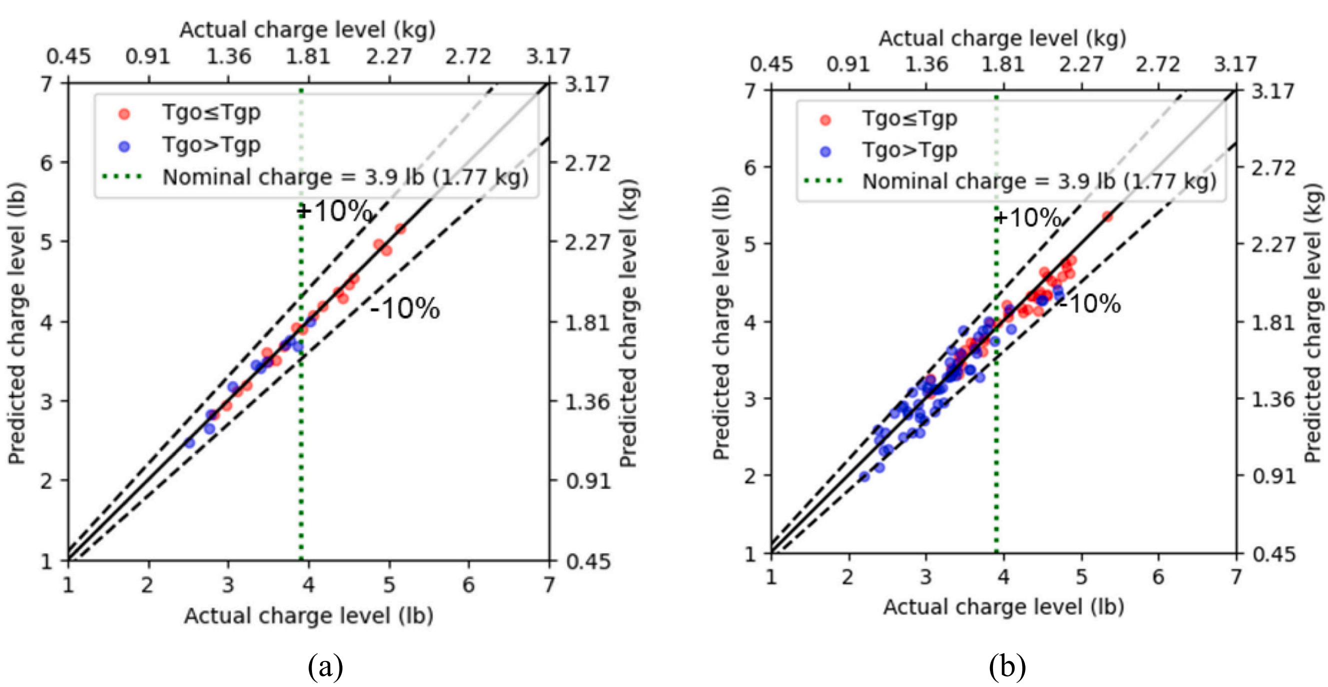

Fig. 13. Reference algorithm 2's performance: (a) training; (b) testing.

Table 10
Test MAPEs under different training data sample sizes.

Algorithm	Training data size of 20	Training data size of 30	Training data size of 50	Training data size of 100
Developed	3.65%	2.57%	2.42%	2.41%
Reference 1	12.05%	4.82%	3.01%	2.59%
Reference 2	5.24%	3.97%	3.61%	3.75%

20, the developed method achieves a MAPE of 3.65%, significantly lower than 12.05% for reference algorithm 1 and 5.24% for reference algorithm 2. When the training sample size is 30 and 50, reference algorithm 1 exhibits the worst performance among the methods. This can be attributed to its higher model complexity, which leads to overfitting under limited data conditions. As the training sample size increases to 100, the performance of reference algorithm 1 improves significantly and eventually surpasses that of reference algorithm 2. A minimum training size of ~30 samples is sufficient to obtain a stable and accurate feature set for the proposed physics-guided, low-complexity (linear) VRC formulation. These results provide valuable guidance for future advancements based on these experimental results.

Moreover, because the training subsets were drawn randomly from the same simulation operating envelope, they may differ in how well they cover the feature/charge regimes. Therefore, this analysis addresses not only the effect of sample count, but also how stable feature selection and prediction accuracy are when the smallest datasets are still representative (without being purposely selected to avoid extrapolation).

4.5. Limitation

It should be noted that the proposed method does not aim to derive a fixed, system-specific equation. Instead, it provides a generalized linear formulation with a set of candidate features. A feature selection process, guided by physical consistency and statistical significance, is applied to identify the most relevant variables for a given system. As a result, the final model structure is adaptively determined, enabling the method to be applicable across different heat pump configurations.

In the current study, a limitation is that it primarily focuses on simulation work. However, the simulation data used in this study are generated based on the HPDM model, which is developed according to fundamental heat pump principles and has been extensively validated using experimental data from heat pump systems operating with common refrigerants. In addition, the purpose of this paper is not to derive a finalized industrial equation for a specific CO_2 heat pump, but to establish a physics-guided feature selection framework for virtual refrigerant charge sensing. The simulation results serve as a consistent platform for comparing the developed algorithm with reference algorithms. Since all algorithms are trained and tested on the same dataset, the comparative analysis remains internally consistent.

Another issue is that the training and testing datasets in this study are generated from the HPDM simulation model. This setup may introduce model bias: the learned regression relationships and the reported errors may reflect HPDM's assumptions and component correlations rather than the exact behavior of an installed residential CO_2 heat pump. Nevertheless, HPDM is a physics-based platform whose modeling framework has been previously validated against experimental measurements for heat pump systems. In addition, the proposed VRC feature selection constrains the final linear model using both statistical significance and physical consistency (expected coefficient sign), which reduces the risk of learning purely HPDM-specific artifacts.

Furthermore, though some previous studies have shown that the VRC sensor is insensitive to the presence of other faults, the performance has not been studied on CO_2 heat pumps. For future work, we plan to evaluate the performance of the VRC sensor on CO_2 heat pumps under the presence of multiple simultaneous faults, such as refrigerant undercharge combined with compressor valve leakage, or evaporator and condenser fouling. Future research will utilize experimental data to rigorously test the algorithm's performance. By validating the algorithm under actual operating conditions, the authors aim to ensure its robustness and reliability for practical applications, addressing challenges related to refrigerant leakage and system performance.

5. Conclusion

VRC sensing technology has been successfully implemented in conventional refrigerant heat pumps. However, its application to CO_2 heat pumps remains limited due to the lack of systematic feature selection methods. This study developed and evaluated a physics-guided feature-selection framework for virtual refrigerant charge sensing using a residential CO_2 heat pump water heater as a case study.

The main research findings are as follows:

1) Among the six candidate features, gas cooler outlet density, evaporator pressure, and superheat temperature are identified as the most relevant features for refrigerant charge prediction in the studied residential CO_2 heat pump.
2) The developed algorithm achieves a testing MAPE below 3%, representing reductions of 46.7% and 35.3% compared with two recent reference VRC algorithms for transcritical CO_2 heat pumps. The improved accuracy is attributed to the selection of physically consistent and statistically significant features, which reduces multicollinearity and overfitting.
3) The effect of training data size is investigated, and a minimum training dataset of approximately 30 samples is found to be sufficient for stable feature selection and satisfactory prediction accuracy.

Declaration of competing interest

The authors declare that they have no known competing financial interests or personal relationships that could have appeared to influence the work reported in this paper.

Acknowledgment

This work was supported by the U.S. Department of Energy, Office of Critical Minerals and Energy Innovation under Lawrence Berkeley National Laboratory Contract No. DE-AC02-05CH11231.

Data availability

Data will be made available on request.

References

[1] S. Jiang, H. Zhao, L. Ni, Review and prospect of air source heat pump research: a bibliometric insight, Int. J. Refrig. 170 (2025) 172–191.
[2] F. Guo, D. Kim, B. Shen, P. Hlanze, J. Cai, Seasonal performance evaluation of zero-superheat active refrigerant charge control for variable-speed heat pumps, Energ. Buildings 351 (2025) 116663.
[3] J. Choi, Y.C. Kim, The effects of improper refrigerant charge on the performance of a heat pump with an electronic expansion valve and capillary tube, Energy 27 (4) (2002) 391–404.
[4] M. Kim, M.S. Kim, Performance investigation of a variable speed vapor compression system for fault detection and diagnosis, Int. J. Refrig. 28 (4) (2005) 481–488.
[5] W. Kim, J.E. Braun, Evaluation of the impacts of refrigerant charge on air conditioner and heat pump performance, Int. J. Refrig. 35 (7) (2012) 1805–1814.
[6] Y. Hu, D.P. Yuill, A. Ebrahimifakhar, A. Rooholghodos, An experimental study of the behavior of a high efficiency residential heat pump in cooling mode with common installation faults imposed, Appl. Therm. Eng. 184 (2021) 116116.
[7] S. Tassou, I. Grace, Fault diagnosis and refrigerant leak detection in vapour compression refrigeration systems, Int. J. Refrig. 28 (5) (2005) 680–688.

[8] H. Rasmussen, S. Thorud, Using a refrigerant leak detector to monitor waste gases from halogenated anesthetics, J. Am. Assoc. Lab. Anim. Sci. 46 (5) (2007) 64–68.
[9] H. Li, J.E. Braun, Development, evaluation, and demonstration of a virtual refrigerant charge sensor, Hvac&R Research 15 (1) (2009) 117–136.
[10] W. Kim, J.E. Braun, Extension of a virtual refrigerant charge sensor, Int. J. Refrig. 55 (2015) 224–235.
[11] W. Kim, J.-H. Lee, Fault detection and diagnostics analysis of air conditioners using virtual sensors, Appl. Therm. Eng. 191 (2021) 116848.
[12] W. Kim, J.E. Braun, Development, implementation, and evaluation of a fault detection and diagnostics system based on integrated virtual sensors and fault impact models, Energ. Buildings 228 (2020) 110368.
[13] Y. Hu, Y. Zhang, X. Liu, H. Li, Development and demonstration of a method to detect refrigerant charge level for variable refrigerant volume systems, Appl. Therm. Eng. 235 (2023) 121354.
[14] G. Li, Y. Hu, H. Chen, L. Shen, H. Li, J. Li, W. Hu, Extending the virtual refrigerant charge sensor (VRC) for variable refrigerant flow (VRF) air conditioning system using data-based analysis methods, Appl. Therm. Eng. 93 (2016) 908–919.
[15] X. Zhu, Z. Du, Z. Chen, X. Jin, X. Huang, Hybrid model based refrigerant charge fault estimation for the data centre air conditioning system, Int. J. Refrig. 106 (2019) 392–406.
[16] S. Boahen, K.H. Lee, J.M. Choi, Refrigerant charge fault detection and diagnosis algorithm for water-to-water heat pump unit, Energies 12 (3) (2019) 545.
[17] F. Guo, D. Kim, P. Hlanze, J. Cai, Rigorous Feature Selection of the Virtual Refrigerant Charge Sensor for Variable-Speed Heat Pumps, in: International Refrigeration and Air Conditioning Conference, 2024. Paper 2661.
[18] Y. Ying, M. Cui, Y. Zhou, W. Shi, B. Wang, Refrigerant substitution pathways of VRF air-conditioning system oriented to Kigali amendment in China, Energ. Buildings 357 (2026) 117138.
[19] C. Liang, F. Guo, D. Kim, P. Hlanze, J. Cai, Virtual refrigerant charge sensor for variable-speed heat pumps based on feature selection, Appl. Therm. Eng. 293 (2026) 130290.
[20] X. Cui, W. Liu, J. Yang, Investigation on the performance potential of a novel heat pump water heater based on transcritical CO2 quasi-two-stage compression with ejector, Int. J. Refrig. 181 (2025) 126–141.
[21] P. Gullo, Innovative fully integrated transcritical R744 refrigeration systems for a HFC-free future of supermarkets in warm and hot climates, Int. J. Refrig. 108 (2019) 283–310.
[22] D. Wang, Y. Lu, L. Tao, Optimal combination of capillary tube geometry and refrigerant charge on a small CO_2 water-source heat pump water heater, Int. J. Refrig. 88 (2018) 626–636.
[23] F. Jia, X. Yin, F. Cao, J. Fang, A. Wang, X. Wang, L. Yang, A novel control method for the automotive CO2 heat pumps under inappropriate refrigerant charge conditions, Energy 286 (2024) 129533.
[24] C. Zhang, B. Hou, M. Li, C. Dang, H. Tong, X. Li, Z. Han, Refrigerant charge estimation method based on data-physic hybrid-driven model for the fault diagnosis of transcritical CO2 heat pump system, Energy 309 (2024) 133144.
[25] DOE/ORNL Heat Pump Design Model. https://hpdmflex.ornl.gov/hpdm/wizard/welcome.php.
[26] F. Anees, B. Shen, J.A. Prem Anand Jayaprabha, X. Liu, An economic and technical feasibility analysis of a dual-source heat pump using both the air and the ground, Energ. Buildings 351 (2025) 116713.
[27] M. Kim, Y.J. Baik, S.R. Park, K.C. Chang, H.S. Ra, Design of a high temperature production heat pump system using geothermal water at moderate temperature, Curr. Appl. Phys. 10 (2) (2010) S117–S122.
[28] R. Bergamini, J.K. Jensen, B. Elmegaard, Thermodynamic competitiveness of high temperature vapor compression heat pumps for boiler substitution, Energy 182 (2019) 110–121.
[29] F. Poggi, H. Macchi-Tejeda, D. Leducq, A. Bontemps, Refrigerant charge in refrigerating systems and strategies of charge reduction, Int. J. Refrig. 31 (3) (2008) 353–370.
[30] J. Braun, S. Klein, J. Mitchell, Effectiveness models for cooling towers and cooling coils, ASHRAE Transactions (American Society of Heating, Refrigerating and Air-Conditioning Engineers);(USA) 95(CONF-890609–), 1988.
[31] C. Liang, W. Wang, H. Wang, X. Li, Year-round energy-efficient multi-stage fresh air treatment system utilizing lake water as energy source, Renew. Energy 247 (2025) 123089.
[32] F.W. Dittus, L.M.K. Boelter, Heat transfer in automobile radiators of the tubular type, Univ. of California Pub., Eng. 2 (13) (1930) 443–461.
[33] A. Standard, Performance rating of unitary air-conditioning & air-source heat pump equipment, AHRI Standard 210/240, 2020.